Journal of Optics

PAPER • OPEN ACCESS

Nonlinear chiral molecular photonics using twisted light: hyper-Rayleigh and hyper-Raman optical activity

To cite this article: Kayn A Forbes 2020 *J. Opt.* **22** 095401

OPEN ACCESS
IOP Publishing
Journal of Optics
J. Opt. **22** (2020) 095401 (12pp)
https://doi.org/10.1088/2040-8986/aba0fd

Nonlinear chiral molecular photonics using twisted light: hyper-Rayleigh and hyper-Raman optical activity

Kayn A Forbes

School of Chemistry, University of East Anglia, Norwich, Norfolk NR4 7TJ, United Kingdom

E-mail: k.forbes@uea.ac.uk

Received 28 April 2020, revised 10 June 2020
Accepted for publication 29 June 2020
Published 28 July 2020

Abstract

Chiroptical and optical activity effects involve differential interactions between matter and light. Generally this involves chiral molecules absorbing or scattering right- and left-handed circularly polarized photons at different rates due to the chiroptical interplay of molecular and optical chirality. Laser light which propagates with a helical phase and twisted wavefront possesses optical orbital angular momentum. These optical vortices can twist either clockwise or anticlockwise, and as such they exhibit an optical handedness or chirality completely distinct from that of circular polarization. It has recently been established that the linear optical effects of single-photon absorption and scattering can exhibit optical activity and chiroptical interactions with respect to the optical vortex handedness. Here a fundamental mechanism of optical activity for twisted light is exhibited in nonlinear processes, with specific emphasis on hyper-Rayleigh and hyper-Raman scattering. In comparison to unstructured or plane-wave light, it is shown that using twisted photons produces novel scattering mechanisms dependent on parameters unique to optical vortex beams. Specifically, the scattered intensity for both hyper-Rayleigh and hyper-Raman optical activity is dependent on the sign and magnitude of the OAM of the incident twisted photons, as well as the transverse position of the chiral scatterer. Moreover, symmetry analysis reveals that, unlike the recently discovered linear optical activity effects with optical vortices, nonlinear scattering of twisted light by chiral molecules leads to a modification of scattering through uniquely weighted individual hyperpolarizability contributions.

Supplementary material for this article is available online

Keywords: optical activity, chirality, structured light, optical vortex, nonlinear optics, hyper-Rayleigh scattering, Raman scattering

(Some figures may appear in colour only in the online journal)

1. Introduction

Nonlinear optics and photonics encompass light-matter interactions that depend on incident electric $\boldsymbol{e}$ and magnetic $\boldsymbol{b}$ fields nonlinearly, such as multi-photon absorption and harmonic generation [1, 2]. hyper-Rayleigh and hyper-Raman scattering are the nonlinear analogues of their respective linear counterparts, Rayleigh (elastic) and Raman (inelastic) scattering [3]. Linear scattering is a two-photon process, where a single input photon of frequency ω is annihilated at the molecule, followed by the creation of an output photon ω'. In Rayleigh scattering $\omega = \omega'$ and the state of scatterer is left unchanged, whereas in the Raman process the light is either Stokes or anti-Stokes shifted $\omega \neq \omega'$, with the molecule in a final state that is different to its initial sate. In the mechanism

of nonlinear scattering, two input photons from an intense laser are annihilated and a single photon is emitted; for hyper-Rayleigh $2\omega = \omega'$, whereas for hyper-Raman $2\omega \neq \omega'$. The similarity of these nonlinear scattering processes to that of coherent second harmonic generation (SHG) sees them often referred to as second harmonic scattering [3]—indeed, hyper-Rayleigh scattering is the incoherent (non-forward) part of second harmonic generation.

Nonlinear scattering is an important tool in laser spectroscopy as it can be a source of molecular information not accessible in either absorption or linear scattering spectra [4]. This stems from the unique selection rules that are determined by the symmetry properties of the hyperpolarizability tensor, the molecular property responsible for the process of nonlinear scattering. Moreover, nonlinear scattering also serves as a widely used method to measure the first (electric dipole) hyperpolarizability tensor of molecules in solution [5]. It is well known that coherent SHG is generally precluded in isotropic fluids to all multipolar orders [6]. hyper-Rayleigh scattering has recently been discovered as a highly useful technique to characterize the nonlinear optical properties of metallic nanoparticles [7] and probe structural correlations in liquids [8, 9].

In 1979 Andrews and Thirunamachandran published theoretical work that highlighted a hyper-Rayleigh and hyper-Raman form of optical activity [10]. Optical activity is the property for a material to exhibit a differential interaction with either left- or right-handed circularly polarized light [11]. The most encountered and general form of optical activity is exhibited by chiral molecules: a right-handed enantiomer interacts with a right-handed circularly polarized photon differently than its left-handed enantiomeric partner. One of the most established types of this chiroptical interaction is circular dichroism: the differential absorption of circularly polarized light by chiral molecules. Another of particular relevance to us here is Rayleigh and Raman optical activity—that is, the differential linear scattering of right- and left-handed photons by chiral molecules [12]. Of these, Raman optical activity has seen particularly profound application in chiroptical spectroscopy [13, 14] since its discovery in the early 1970s. This stems from its ability to probe the invariably chiral biomolecules found in nature using visible light, to a high degree, due to the fact it provides rich information on vibrational structure associated with the $3n$–6 degrees of vibrational freedom of molecules consisting of n atoms [15–18]. *Nonlinear* optical activity [19] is an important spectroscopic method due to the unique characteristics afforded to it by the quadratic or higher dependence on the incident electromagnetic fields. Specifically, it can be used to study the dynamics of chiral and biological molecules at ultrafast timescales, act as an incisive probe of surface chirality, and yield chiroptical observables many orders of magnitudes larger than linear optical activity effects [20–24]. Such advantages are also now being realized in the nonlinear spectroscopy and imaging of metamaterials [25].

It was the lack of sufficiently intense laser sources that initially rendered observation of hyper-Rayleigh and hyper-Raman scattering difficult, and observing the even weaker effect of hyper-Rayleigh and hyper-Raman optical activity occurred four decades after the original theory was published. In their work, Collins *et al* [26]. took advantage of the plasmonic enhancement of optical interactions which arise for metallic nanoparticles interacting with light, to observe hyper-Rayleigh optical activity of an isotropic solution of silver nanohelices in water. Soon after a group in France managed to observe hyper-Rayleigh optical activity with molecular matter [27]. Observing hyper-Raman optical activity is being actively pursued [28], the attractiveness of this form of nonlinear optical activity is the much larger amount of chiral structural information that can be obtained for to similar reasons as its linear analogue, ROA.

To date, all studies of hyper-Rayleigh and hyper-Raman optical activity have utilized the differential interactions between the chiral molecules and input circularly polarized light. The circularly polarized states, originating from the spin angular momentum (SAM) of photons, constitute the most well-known form of optical chirality or handedness. However, light that is suitably structured so as to propagate with helical wavefronts also possess a form of chirality or handedness that is completely distinct from the polarization (figure 1). These optical vortices, or twisted light beams, carry well-defined orbital angular momentum (OAM) in the propagation direction of $\pm\ell\hbar$ per photon, where ℓ is known as the topological charge and signifies the number of entwined helicoidal wavefront surfaces [29–31]. This optical OAM of laser beams has seen profound application in a plethora of areas [32]: optical manipulation [33]; optical communications [34]; atomic optics and spectroscopy [35]; fabricating chiral nanostructures [36]; and even revealing deep insights into entanglement and quantum optics [37]. In addition, optical OAM has also been extensively studied in the field of nonlinear optics and photonics, with a strong emphasis on the coherent harmonic generation of optical vortices through frequency conversion [38, 39] and wave-mixing mechanisms [40–42].

The sign of the topological charge (and OAM) ℓ determines what direction (clockwise or anticlockwise) these optical vortices twist: $\ell > 0$ are left-handed, $\ell < 0$ right-handed. It is therefore natural to ask the question of whether materials can exhibit optical activity due to the handedness associated with these optical vortices. Whilst the first studies looking at this issue were published nearly two decades ago, this field of twisted light and optical activity has seen significant research effort in the last few years due to significant advances in the underlying theoretical comprehension of the mechanisms at play [43–47].

In this work the first example of nonlinear optical activity with twisted light is presented. Specifically, it is shown that both hyper-Rayleigh and hyper-Raman scattering by a chiral molecule is dependent on the handedness of an incident optical vortex laser beam. It is discovered that not only does the scattered intensity depend on the sign of the topological charge of the input photons, it also depends on their magnitude, with photons possessing high OAM values increasing the measured scattered optical activity signals. We begin in section 2 with a quantum electrodynamical derivation of the quantum amplitude (matrix element) for the hyper-Rayleigh

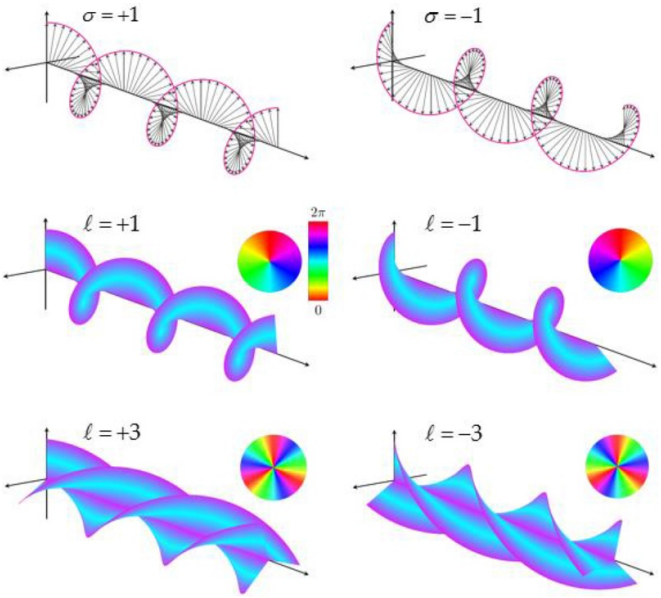

Figure 1. Optical chirality. (Top) Left-handed circularly polarized light (left); right-handed circularly polarized light (right). Electromagnetic field vectors trace out a chiral helical structure on propagation in circularly polarized light, giving it a handedness. (Bottom) Optical vortex beams twisting to the left (anticlockwise) and to the right (clockwise). Both forms of handedness are defined from the point of view of the receiver.

scattering of twisted photons; section 3 takes the quantum amplitude and uses it to derive the experimentally observable scattered intensity of twisted photons for both oriented molecules and randomly oriented chiral molecules; section 4 develops the general scattered intensity from section 3 into the specific scattered intensity difference for input circularly polarized twisted photons for an arbitrary scattering angle, and it is seen that this measurable difference in scattered intensity is dependent on ℓ; section 5 exhibits how the results of the previous Sections are easily adapted to account for hyper-Raman scattering of twisted photons, and also discusses the unique property that nonlinear scattering of twisted photons has on the relative contributions from specific polarizability contributions to the transition rates and scattered intensity differential; section 6 concludes the analysis by highlight future avenues the work can be taken down.

2. Quantum amplitude for the nonlinear scattering of twisted photons

To derive the intensity of twisted light scattered by a chiral molecule we utilize molecular quantum electrodynamics (MQED) [48, 49]. In contrast to semi-classical methods where the radiation is treated as a classical wave, MQED treats the total light-matter system, including the electromagnetic field, in a full quantum framework, and thus represents the true nature of light-matter interactions in terms of photons [50].

We start with the Power-Zienau-Woolley system Hamiltonian operator [51] $H = (H_{\rm mol} + H_{\rm rad}) + H_{\rm int}$, where $H_{\rm mol}$ is the molecular Hamiltonian operator and $H_{\rm rad}$ is the Hamiltonian operator for the radiation field. The final operator is the interaction Hamiltonian $H_{\rm int}$, which perturbs the system, allowing transitions between the eigenstates of $(H_{\rm mol} + H_{\rm rad})$:

$$H_{\rm int} = -\varepsilon_0^{-1}\mu_i d_i^{\perp} - \varepsilon_0^{-1} Q_{ij}\nabla_j d_i^{\perp}\cdots, -m_i b_i\cdots, \qquad (1)$$

where $\boldsymbol{\mu}$ and $\boldsymbol{Q}$ are the electric dipole and electric quadrupole moment operators, respectively, and $\boldsymbol{m}$ is the magnetic dipole moment operator; $\boldsymbol{d}^{\perp}$ is the transverse electric displacement field operator, $\boldsymbol{b}$ is the magnetic field operator; Einstein summation of repeated tensor indices is assumed throughout this work. In our analysis we will center on the paraxial Laguerre–Gaussian modes of twisted light, whose quantized mode expansion is given by [52]

$$\boldsymbol{d}^{\perp}(\boldsymbol{r}) = i\sum_{k,\eta,\ell,p}\left(\frac{\hbar ck\varepsilon_0}{2A_{\ell,p}^2 V}\right)^{1/2}[\boldsymbol{e}^{(\eta)}(k\hat{\boldsymbol{z}})\,a_{\ell,p}{}^{(\eta)}(k\hat{\boldsymbol{z}})f_{|\ell|,p}(r)\,{\rm e}^{(ikz+i\ell\phi)} - \bar{\boldsymbol{e}}^{(\eta)}(k\hat{\boldsymbol{z}})\,a_{\ell,p}{}^{\dagger(\eta)}(k\hat{\boldsymbol{z}})\bar{f}_{|\ell|,p}(r)\,{\rm e}^{-(ikz+i\ell\phi)}], \qquad (2)$$

where $A_{\ell,p}$ is a normalization constant; V is the quantization volume; $f_{|\ell|,p}(r)$ is a radial distribution function of the beam (it is independent of the sign of ℓ); $\boldsymbol{e}^{(\eta)}(k\hat{\boldsymbol{z}})$ is the electric field polarization unit vector dependent on the wave vector $k\hat{\boldsymbol{z}}$; $a_{\ell,p}^{(\eta)}(k\hat{\boldsymbol{z}})$ and $a_{\ell,p}^{\dagger(\eta)}(k\hat{\boldsymbol{z}})$ are LG photon creation and annihilation operators; and ${\rm e}^{(ikz+i\ell\phi)}$ is the phase factor. It is this azimuthal phase factor ${\rm e}^{i\ell\phi}$ which gives LG beams their orbital angular momentum [29]. The quantum operator for the magnetic field $\boldsymbol{b}$ takes on an analogous form to (2).

The multipolar expansion (1) includes the two leading terms dependent on the electric field—electric dipole (E1) and electric quadrupole (E2) interactions—as well as the leading magnetic interaction (magnetic dipole) M1. The E1 interaction is generally three orders of magnitude larger than both M1 and E2 interaction terms, of which both are similar in coupling strength. Optical activity effects in chiral molecules generally stem from interferences of E1 with both the weaker E2 and M1 [11]. However, it has now been very well established [46] that any dependence on the topological charge (and thus the vortex handedness) of a twisted light beam can only stem from E2 interactions (to this level of multipolar approximation), and therefore to make the calculations easy to follow we neglect M1 interactions as there is nothing novel in their interactions with optical OAM [46, 53, 54]. However, it must be made clear that circularly polarized twisted light will still produce optical activity effects that depend on E1 and M1 interferences, but these are the well-known forms of circular differential optical activity due to the optical helicity. Of course, in the pursuit of quantitative congruence between the results presented here and the observations of experiments these must be included.

Our analysis will centre on hyper-Rayleigh scattering, where $2k = k'$ but $\hat{\boldsymbol{k}} \neq \hat{\boldsymbol{k}}'$, in the knowledge that hyper-Rayleigh scattering and optical activity is easily extended using textbook methods [12] to account for hyper-Raman scattering $2k \neq k'$ (as we go on to show in section 5). An initial system state consisting of a chiral molecule ξ subjected to a Laguerre–Gaussian beam containing n photons of the mode

(k,η,ℓ,p) takes the form $|i\rangle = |E_0(\xi)\rangle|n(k,\eta,\ell,p)\rangle$. During the hyper-Rayleigh scattering process two input photons are annihilated at the chiral molecule, and a single output photon of some scattered mode $(\boldsymbol{k}',\eta')$ is created, which in the general case has an indeterminable angular momentum for molecular scattering [55] (though the theory readily accommodates the possibility of specific scattered modes, including twisted photons [56]). This final state is given by $|f\rangle = |E_0(\xi)\rangle|(n-2)(k,\eta,\ell,p);1((\boldsymbol{k}',\eta'))\rangle$.

The matrix element for the nonlinear scattering processes can be calculated using third-order time-dependent perturbation theory:

$$M_{fi} = \sum_{r,s} \frac{\langle f|H_{\rm int}|s\rangle\langle s|H_{\rm int}|r\rangle\langle r|H_{\rm int}|i\rangle}{(E_i - E_s)(E_i - E_r)}, \tag{3}$$

where $H_{\rm int}$ is given by the first two terms in (1). The computation of intermediate states r and s in (3) is made decidedly clearer using the time-ordered Feynman diagrams in figure 2. The matrix element for solely E1 interactions, 'E1E1E1' or E1 [3], which corresponds to standard hyper-Rayleigh scattering is

$$M_{fi}^{\rm E1^3} = -i\sum_{\boldsymbol{k}',\eta'}\left(\frac{\hbar ck}{2\varepsilon_0 V}\right)^{\frac{3}{2}}\left(\frac{n(n-1)}{A_{\ell,p}^4}\right)^{\frac{1}{2}} f_{|\ell|,p}^2(r)\,\overline{e'}_i^{(\eta')}(\boldsymbol{k}')\,e_j^{(\eta)} (k\hat{\boldsymbol{z}})\,e_k^{(\eta)}(k\hat{\boldsymbol{z}})\,\beta_{ijk}^{00}(-2\omega;\omega,\omega,)\,{\rm e}^{2ikz}{\rm e}^{2i\ell\phi}{\rm e}^{-i\boldsymbol{k}'\cdot\boldsymbol{r}}, \tag{4}$$

where $\beta_{ijk}^{00}(-2\omega;,\omega,\omega,)$ is the hyperpolarizability tensor defined as

$$\beta_{ijk}^{00}(-2\omega;\omega,\omega,) = \frac{1}{2}\sum_{r,s}\left[\left\{\frac{\mu_i^{0s}\mu_j^{sr}\mu_k^{r0}}{(E_{s0}-2\hbar\omega)(E_{r0}-\hbar\omega)} + \frac{\mu_j^{0s}\mu_i^{sr}\mu_k^{r0}}{(E_{s0}+\hbar\omega)(E_{r0}-\hbar\omega)} + \frac{\mu_j^{0r}\mu_k^{rs}\mu_i^{s0}}{(E_{s0}+\hbar\omega)(E_{r0}+2\hbar\omega)} + \{j\leftrightarrow k\}\right\}\right], \tag{5}$$

where $E_{s0} = E_s - E_0$.

The inclusion of a single E2 interaction leads to the three distinct E1 [2] E2′, E1E2E1′ and E2E1E1′ contributions to the total matrix element, with a prime indicating the multipole moment engaged in the photon emission step. The inclusion of all these possibilities is a necessity of the QED framework. With the aid of the Feynman diagrams in figure 3, the total matrix element for these interactions is found to be

$$M_{fi}^{\rm E1E1E2} = -i\sum_{\boldsymbol{k}',\eta'}\left(\frac{\hbar ck}{2\varepsilon_0 V}\right)^{\frac{3}{2}}\left(\frac{n(n-1)}{A_{\ell,p}^4}\right)^{\frac{1}{2}} f_{|\ell|,p}^2(r)\,\overline{e'}_i e_j e_k \left[\left(i\frac{\ell}{r}\hat{\phi}_l + ik\hat{z}_l\right)\chi_{ijkl}^{00} - ik'\hat{k}'_l\chi_{ijkl}^{00}\right]{\rm e}^{2ikz}{\rm e}^{2i\ell\phi}{\rm e}^{-i\boldsymbol{k}'\cdot\boldsymbol{r}}, \tag{6}$$

where we have dropped polarization vector dependencies for brevity; $k'\hat{\boldsymbol{k}}' = \boldsymbol{k}'$; and the 4th rank polarizability tensors are defined as:

$$\chi'^{00}_{ijkl}(-2\omega;\omega,\omega) = \tfrac{1}{2}\sum_{r,s}[\{\tfrac{Q_{il}^{0s}\mu_j^{sr}\mu_k^{r0}}{(E_{s0}-2\hbar\omega)(E_{r0}-\hbar\omega)} + \tfrac{\mu_j^{0s}Q_{il}^{sr}\mu_k^{r0}}{(E_{s0}+\hbar\omega)(E_{r0}-\hbar\omega)} + \tfrac{\mu_j^{0s}\mu_k^{sr}Q_{il}^{r0}}{(E_{s0}+\hbar\omega)(E_{r0}+2\hbar\omega)}\} + \{j\leftrightarrow k\}]. \tag{7}$$

and

$$\chi_{ijkl}^{00}(-2\omega;\omega,\omega) = \chi^{a}{}_{ijkl}(-2\omega;\omega,\omega) + \chi^{b}{}_{ikjl}(-2\omega;\omega,\omega) = \sum_{r,s}\left\{\frac{\mu_i^{0s}Q_{jl}^{sr}\mu_k^{r0}}{(E_{s0}-2\hbar\omega)(E_{r0}-\hbar\omega)} + \frac{Q_{jl}^{0s}\mu_i^{sr}\mu_k^{r0}}{(E_{s0}+\hbar\omega)(E_{r0}-\hbar\omega)} + \frac{Q_{jl}^{0s}\mu_k^{sr}\mu_i^{r0}}{(E_{s0}+\hbar\omega)(E_{r0}+2\hbar\omega)} + \frac{\mu_i^{0s}\mu_k^{sr}Q_{jl}^{r0}}{(E_{s0}-2\hbar\omega)(E_{r0}-\hbar\omega)} + \frac{\mu_k^{0r}\mu_i^{sr}Q_{jl}^{r0}}{(E_{s0}+\hbar\omega)(E_{r0}-\hbar\omega)} + \frac{\mu_k^{0s}Q_{jl}^{sr}\mu_i^{r0}}{(E_{s0}+\hbar\omega)(E_{r0}+2\hbar\omega)}\right\}. \tag{8}$$

The χ'_{ijkl} polarizability tensor has both j, k and i, l index symmetry, stemming from identical input photons and the symmetric property of the quadrupole transition moment in the E1^{2}E2′ contribution. The χ_{ijkl} polarizability is j, l-symmetric.

We may already observe at this early stage of the calculation that (6) has terms that are linearly dependent on ℓ, and thus the wavefront handedness of the vortex. It is instructive to explicitly highlight where this dependence stems from in the E2 coupling:

$$\nabla_j\tilde{d}_i^{\perp} \propto e_i\left(\frac{1}{r}\frac{\partial}{\partial\phi}\hat{\phi}_j + \frac{\partial}{\partial z}\hat{z}_j\right)f_{\ell,p}(r)\,{\rm e}^{(ikz+i\ell\phi)} = e_i\left(\frac{i\ell\hat{\phi}_j}{r} + ik\hat{z}_j\right)f_{\ell,p}(r)\,{\rm e}^{(ikz+i\ell\phi)}, \tag{9}$$

where we have neglected the $\partial/\partial r$ terms as these do not engage with the phase, and thus cannot engage optical chirality. It is clearly necessary for materials (atomic, molecular, or otherwise) to engage in interactions which couple to the gradient of the electromagnetic field in order to observe non-mechanical effects dependent directly on optical OAM. In the multipolar expansion, it is the E2 interaction at which this occurs to the lowest order, and therefore in general most experimentally significant: higher order interactions engage the gradient of the fields, but these only diminish in magnitude for most scenarios. Importantly, for molecular matter, it is the E1E2 interference cross-terms at lowest order to which these interactions can therefore occur. This is obviously not the case in atoms, where the system must engage solely E2 transitions to the lowest order of coupling [43, 45]. In order to exhibit E1E2 interactions in isotropic molecular systems, the constituent molecules must be of the correct symmetry: these require a chiral structure—but it is the gradient of the field which is the paradigm feature in light-matter interactions in order to engage the optical OAM of photons in spectroscopic applications [57, 58].

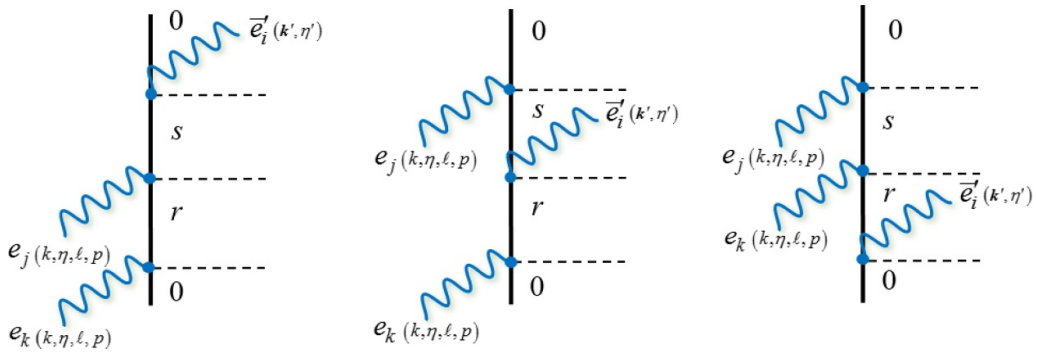

Figure 2. Three topologically distinct Feynman graphs for hyper-Rayleigh scattering used in the calculation of the hyperpolarizability β_{ijk}^{00}. Time progresses upwards, space is characterized by the horizontal axis. Wavy lines represent E1 photon interactions at the molecule (vertical line), where the molecule progresses from the ground state 0, through intermediate states r and s.

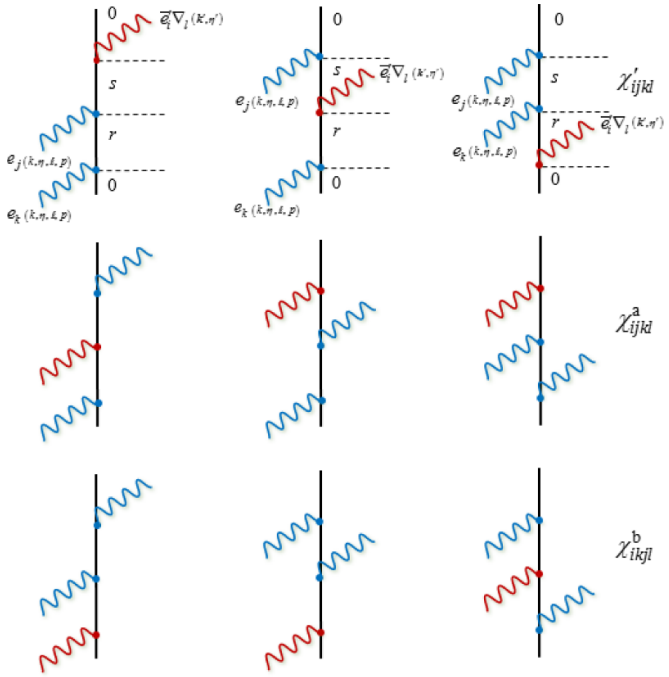

Figure 3. Nine (three sets of three grouped horizontally) topologically distinct Feynman diagrams needed in the calculation of (6). Diagrams to be interpreted the same as in figure 2, except red wavy lines represent E2 photon couplings to the molecule. Each set of three horizontal Feynman pathways produce the respective polarizability tensor χ in equations (7) and (8) shown to the right.

3. Scattered intensity of twisted photons

In order to calculate the scattered intensity of circularly polarized twisted light, the experimental measurable we are most interested in, we must invoke the Fermi rate rule as standard which allows us to write the scattered radiant intensity (the amount of energy emitted per unit solid angle per unit time) as [48]

$$I'(\boldsymbol{k}') = k^3 V \left\langle \left| \sum_{\xi} M_{fi}(\xi) \right|^2 \right\rangle (4\pi^2\hbar)^{-1}, \qquad (10)$$

where angular brackets denote molecular orientational averaging, and M_{fi} is the total quantum amplitude i.e. the sum of (4) and (6). Carrying out the calculation gives for the scattered radiant intensity

$$I'(\boldsymbol{k}') = \frac{N_r \bar{I}^2(r) g^{(2)} k^4}{16c\pi^2\varepsilon_0^3} \bar{e'}_i e_j e_k e'_l \bar{e}_m \bar{e}_n \left[\frac{1}{2} \langle \beta_{i(jk)} \beta_{lmn} \rangle + ik\hat{k}'_o \langle \beta_{i(jk)} \chi'_{lmno} \rangle - \left(i\frac{\ell}{r}\hat{\phi}_o + ik\hat{z}_o \right) \langle \beta_{i(jk)} \chi_{lmno} \rangle \right]. \qquad (11)$$

where we define the mean input beam irradiance (power per unit area) as $\bar{I}(r) = \langle n \rangle \hbar c^2 k f_{\ell,p}^2(r) / A_{\ell,p}^2 V$ and $g^{(2)}$ is the degree of second-order coherence. Clearly the scattered intensity is dependent on N_r molecules at position r, which shows hyper-Rayleigh scattering is incoherent, unlike the N^2 dependence of coherent scattering (any Raman process is always incoherent). The first term on the left-hand side in the square brackets of (11), dependent on solely the hyperpolarizability tensor $\boldsymbol{\beta}^{00}$, is the leading order, solely electric dipole contribution to hyper-Rayleigh scattering; it is an analogous form to that derived for plane-wave light [48], the minor difference being that it depends on the Laguerre–Gaussian intensity distribution through $\bar{I}^2(r)$. The two cross-terms on the right-hand side of (11) contribute to hyper-Rayleigh optical activity (remembering also that in a full multipolar analysis there are OAM-independent terms stemming from magnetic dipole interactions). The response tensors engaged in sum-frequency generation in a chiral liquid and its static electric field-induced analogue have a similar structure to those in (11), though involve only E1 couplings [59].

At this juncture we may concentrate on the two right-hand terms in square brackets in (11), as we are interested in contributions to the scattering which depend on both molecular chirality and optical chirality: the first term corresponds to the dominant mechanism of hyper-Rayleigh scattering which occurs through solely E1 interactions with the field and exhibits no optical activity. The result (11) as it stands is currently applicable to arrangements of molecules with a fixed orientation with respect to the laboratory frame of reference (e.g. crystaline media). In order for (11) to give the

scattered intensity for molecules that are randomly orientated, as would be the case in a liquid or gas, the three-dimensional rotational average has to be carried out. The standard method of calculation is well established [60], and for low rank molecular tensors is very straightforward. However, the advantage of being able to derive analytical rotationally averaged results is somewhat offset by the fact we require the very involved 7th-rank tensor average scheme to calculate $\left\langle \beta_{ijk}\chi_{lmno}\right\rangle$ and $\left\langle \beta_{ijk}\chi'_{lomn}\right\rangle$ in (11). The full derivation is provided in the supplementary information (available online at stacks.iop.org/JOPT/22/095401/mmedia), but involves contraction of 36 linearly independent isotropic tensor products of a Kronecker delta doublet and a single Levi–Civita referred to the laboratory frame (polarization vector components), and a further 36 tensor products of the same structure for the molecular frame; here the result is broken into three parts: The contribution to the scattered intensity from $\hat{\boldsymbol{z}}$-terms in (11) is

$$I'^{\beta\chi}_{\hat{\boldsymbol{z}}}\left(\boldsymbol{k'}\right)=-\frac{N_r\bar{I}^2\left(r\right)g^{(2)}k^4}{16c\pi^2\varepsilon_0^3}\frac{ik}{420}\begin{pmatrix}\mathrm{a}\\ \mathrm{b}\\ \mathrm{c}\\ \mathrm{d}\\ \mathrm{e}\\ \mathrm{f}\end{pmatrix}^T\begin{pmatrix}-8&4&-8&8&20&-4&0&-10&-4\\ -20&28&-8&-16&20&-20&12&-10&-12\\ 20&-24&20&36&-36&24&-28&18&24\\ 24&-20&6&18&-22&30&-18&15&18\\ -12&12&-10&-18&18&-18&30&-15&-12\\ -16&12&-4&-20&24&-18&12&-12&-24\end{pmatrix}\begin{pmatrix}\mathrm{A}\\ \mathrm{B}\\ \mathrm{C}\\ \mathrm{D}\\ \mathrm{E}\\ \mathrm{F}\\ \mathrm{G}\\ \mathrm{H}\\ \mathrm{I}\end{pmatrix};\quad(12)$$

for $\hat{\boldsymbol{\phi}}$-terms

$$I'^{\beta\chi}_{\hat{\boldsymbol{\phi}}}\left(\boldsymbol{k'}\right)=-\frac{N_r\bar{I}^2\left(r\right)g^{(2)}k^4}{16c\pi^2\varepsilon_0^3}\frac{i\ell r^{-1}}{420}\begin{pmatrix}\mathrm{a}'\\ \mathrm{b}'\\ \mathrm{c}'\\ \mathrm{d}'\\ \mathrm{e}'\\ \mathrm{f}'\\ \mathrm{g}'\\ \mathrm{h}'\\ \mathrm{i}'\\ \mathrm{j}'\\ \boldsymbol{k}'\\ \mathrm{l}'\end{pmatrix}^T\begin{pmatrix}-8&12&-8&-28&20&-16&28&-12&-16\\ 40&-20&0&20&-28&24&-12&20&16\\ 12&-4&4&12&-24&8&-8&12&12\\ -8&4&-8&8&20&-6&0&-10&-4\\ -28&12&8&8&36&-16&4&-18&-20\\ -20&28&-8&-16&20&20&12&-10&-12\\ 20&-24&20&36&-36&24&-28&18&24\\ -16&8&-4&-16&24&-12&12&-18&-18\\ 28&-8&0&8&-28&12&0&30&12\\ 24&-20&6&18&-22&30&-18&15&18\\ -12&12&-10&-18&18&-18&30&-15&-12\\ -16&12&-4&-20&24&-18&12&-12&-24\end{pmatrix}\begin{pmatrix}\mathrm{A}\\ \mathrm{B}\\ \mathrm{C}\\ \mathrm{D}\\ \mathrm{E}\\ \mathrm{F}\\ \mathrm{G}\\ \mathrm{H}\\ \mathrm{I}\end{pmatrix};\quad(13)$$

and for $\hat{\boldsymbol{k}}'$-terms

$$I'^{\beta\chi'}_{\hat{\boldsymbol{k}}'}\left(\boldsymbol{k'}\right)=\frac{N_r\bar{I}^2\left(r\right)g^{(2)}k^4}{16c\pi^2\varepsilon_0^3}\frac{ik}{420}\begin{pmatrix}\mathrm{a}''\\ \mathrm{b}''\\ \mathrm{c}''\\ \mathrm{d}''\\ \mathrm{e}''\\ \mathrm{f}''\\ \mathrm{g}''\\ \mathrm{h}''\\ \mathrm{i}''\end{pmatrix}^T\begin{pmatrix}12&-36&12&28&-84\\ -4&40&-12&-32&76\\ 0&0&24&-16&24\\ -12&-20&36&-4&-36\\ -12&8&-4&4&-20\\ 36&4&-12&4&36\\ 6&10&-6&-6&30\\ -6&-10&6&6&-30\\ -16&-8&16&-12&-24\end{pmatrix}\begin{pmatrix}\mathrm{A}''\\ \mathrm{B}''\\ \mathrm{C}''\\ \mathrm{D}''\\ \mathrm{E}''\end{pmatrix}.\quad(14)$$

Table 1. Scalar molecular invariants for $\beta_{ijk}\chi_{lmno}$ and $\beta_{ijk}\chi'_{lmno}$(Latin indices refer to the laboratory frame, Greek indices refer to the molecular frame).

Molecular tensors	Label	Molecular tensors	Label
$\varepsilon_{\lambda\mu\pi}\beta_{\lambda\mu\rho}\chi_{\pi\sigma\sigma\rho}$	A	$\varepsilon_{\lambda\mu\pi}\beta_{\lambda\mu\rho}\chi'_{\pi\rho\sigma\sigma}$	A′′
$\varepsilon_{\lambda\mu\pi}\beta_{\lambda\mu\rho}\chi_{\rho\pi\sigma\sigma}$	B	$\varepsilon_{\lambda\mu\pi}\beta_{\lambda\mu\rho}\chi'_{\pi\sigma\sigma\rho}$	B′′
$\varepsilon_{\lambda\mu\pi}\beta_{\lambda\mu\rho}\chi_{\sigma\pi\sigma\rho}$	C	$\varepsilon_{\lambda\mu\pi}\beta_{\lambda\mu\rho}\chi'_{\rho\pi\sigma\sigma}$	C′′
$\varepsilon_{\lambda\mu\pi}\beta_{\lambda\mu\rho}\chi_{\sigma\pi\rho\sigma}$	D	$\varepsilon_{\lambda\pi\rho}\beta_{\lambda\mu\mu}\chi'_{\pi\rho\sigma\sigma}$	D′′
$\varepsilon_{\lambda\mu\pi}\beta_{\lambda\mu\rho}\chi_{\sigma\sigma\pi\rho}$	E	$\varepsilon_{\lambda\pi\rho}\beta_{\lambda\mu\nu}\chi'_{\pi\rho\nu\mu}$	E′′
$\varepsilon_{\lambda\pi\rho}\beta_{\lambda\mu\mu}\chi_{\pi\rho\sigma\sigma}$	F	–	–
$\varepsilon_{\lambda\pi\nu}\beta_{\lambda\mu\rho}\chi_{\pi\rho\mu\nu}$	G	–	–
$\varepsilon_{\lambda\pi\nu}\beta_{\lambda\mu\rho}\chi_{\pi\rho\nu\mu}$	H	–	–
$\varepsilon_{\lambda\pi\rho}\beta_{\lambda\mu\mu}\chi_{\sigma\pi\rho\sigma}$	I	–	–

Table 2. Scalar optical invariants for terms dependent on $k\hat{\boldsymbol{z}}$. $\boldsymbol{c} = \boldsymbol{e}\times\bar{\boldsymbol{e}}$ and $\boldsymbol{c}' = \boldsymbol{e}'\times\bar{\boldsymbol{e}}'$.

Optical tensors	Label
$(\boldsymbol{c}\cdot\bar{\boldsymbol{e}}')(\hat{\boldsymbol{z}}\cdot\boldsymbol{e}')$	a
$(\boldsymbol{e}\times\hat{\boldsymbol{z}}\cdot\bar{\boldsymbol{e}}')(\bar{\boldsymbol{e}}\cdot\bar{\boldsymbol{e}})(\boldsymbol{e}\cdot\boldsymbol{e}')$	b
$(\boldsymbol{e}\times\hat{\boldsymbol{z}}\cdot\bar{\boldsymbol{e}}')(\boldsymbol{e}'\cdot\bar{\boldsymbol{e}})$	c
$(\bar{\boldsymbol{e}}'\times\boldsymbol{e}'\cdot\hat{\boldsymbol{z}})(\boldsymbol{e}\cdot\boldsymbol{e})(\bar{\boldsymbol{e}}\cdot\bar{\boldsymbol{e}})$	d
$-(\boldsymbol{c}'\cdot\hat{\boldsymbol{z}})$	e
$(\bar{\boldsymbol{e}}\times\hat{\boldsymbol{z}}\cdot\bar{\boldsymbol{e}}')(\boldsymbol{e}'\cdot\bar{\boldsymbol{e}})(\boldsymbol{e}\cdot\boldsymbol{e})$	f

Table 3. Scalar optical invariants for terms dependent on $\ell r^{-1}\hat{\boldsymbol{\phi}}$.

Optical tensors	Label	Optical tensors	Label
$(\boldsymbol{c}'\cdot\boldsymbol{e})\left(\hat{\boldsymbol{\phi}}\cdot\bar{\boldsymbol{e}}\right)$	a′	$\left(\boldsymbol{e}\times\hat{\boldsymbol{\phi}}\cdot\bar{\boldsymbol{e}}'\right)(\boldsymbol{e}'\cdot\bar{\boldsymbol{e}})$	g′
$(\boldsymbol{c}'\cdot\boldsymbol{e})(\bar{\boldsymbol{e}}\cdot\bar{\boldsymbol{e}})\left(\hat{\boldsymbol{\phi}}\cdot\boldsymbol{e}\right)$	b′	$-(\boldsymbol{c}'\cdot\bar{\boldsymbol{e}})(\boldsymbol{e}\cdot\boldsymbol{e})\left(\hat{\boldsymbol{\phi}}\cdot\bar{\boldsymbol{e}}\right)$	h′
$(\boldsymbol{c}\cdot\bar{\boldsymbol{e}}')(\boldsymbol{e}\cdot\boldsymbol{e}')\left(\hat{\boldsymbol{\phi}}\cdot\bar{\boldsymbol{e}}\right)$	c′	$-(\boldsymbol{c}'\cdot\bar{\boldsymbol{e}})\left(\hat{\boldsymbol{\phi}}\cdot\boldsymbol{e}\right)$	i′
$(\boldsymbol{c}\cdot\bar{\boldsymbol{e}}')\left(\hat{\boldsymbol{\phi}}\cdot\boldsymbol{e}'\right)$	d′	$-\left(\boldsymbol{c}'\cdot\hat{\boldsymbol{\phi}}\right)(\boldsymbol{e}\cdot\boldsymbol{e})(\bar{\boldsymbol{e}}\cdot\bar{\boldsymbol{e}})$	j′
$(\boldsymbol{c}\cdot\bar{\boldsymbol{e}}')(\boldsymbol{e}'\cdot\bar{\boldsymbol{e}})\left(\hat{\boldsymbol{\phi}}\cdot\bar{\boldsymbol{e}}\right)$	e′	$-\left(\boldsymbol{c}'\cdot\hat{\boldsymbol{\phi}}\right)$	k′
$\left(\boldsymbol{e}\times\hat{\boldsymbol{\phi}}\cdot\bar{\boldsymbol{e}}'\right)(\bar{\boldsymbol{e}}\cdot\bar{\boldsymbol{e}})(\boldsymbol{e}\cdot\boldsymbol{e}')$	f′	$\left(\bar{\boldsymbol{e}}\times\hat{\boldsymbol{\phi}}\cdot\bar{\boldsymbol{e}}'\right)(\boldsymbol{e}'\cdot\bar{\boldsymbol{e}})(\boldsymbol{e}\cdot\boldsymbol{e})$	l′

The optical and molecular scalar invariants associated with the alphabetical labels in (12)–(14) are explicitly given in tables 1–4. The total scattered intensity due to $\beta\chi$ scattering is the sum of the real parts of (12)–(14). Clearly the contribution (13) is ℓ-dependent, whilst the other two contributions (12) and (14) are analogous versions for Laguerre–Gaussian beams that represent the quadrupole contribution to hyper-Rayleigh optical activity for unstructured light.

4. Circular-differential scattering and angle dependence

We now develop the general results of the previous section in order to make them clearly and directly relevant to experimental measurements. The most common method of studying optical activity in scattering experiments is measuring the scattered intensity *difference* between input

Table 4. Scalar optical invariants for terms dependent on $k\hat{\boldsymbol{k}}'$.

Optical tensors	Label
$(\boldsymbol{c}'\cdot\boldsymbol{e})\left(\hat{\boldsymbol{k}}'\cdot\bar{\boldsymbol{e}}\right)$	a′′
$(\boldsymbol{c}'\cdot\boldsymbol{e})(\bar{\boldsymbol{e}}\cdot\bar{\boldsymbol{e}})\left(\hat{\boldsymbol{k}}'\cdot\boldsymbol{e}\right)$	b′′
$(\boldsymbol{c}\cdot\bar{\boldsymbol{e}}')(\boldsymbol{e}\cdot\boldsymbol{e}')\left(\hat{\boldsymbol{k}}'\cdot\bar{\boldsymbol{e}}\right)$	c′′
$(\boldsymbol{c}\cdot\bar{\boldsymbol{e}}')(\boldsymbol{e}'\cdot\bar{\boldsymbol{e}})\left(\hat{\boldsymbol{k}}'\cdot\boldsymbol{e}\right)$	d′′
$\left(\hat{\boldsymbol{k}}'\times\bar{\boldsymbol{e}}'\cdot\boldsymbol{e}\right)(\bar{\boldsymbol{e}}\cdot\bar{\boldsymbol{e}})(\boldsymbol{e}\cdot\boldsymbol{e}')$	e′′
$\left(\hat{\boldsymbol{k}}'\times\bar{\boldsymbol{e}}'\cdot\boldsymbol{e}\right)(\boldsymbol{e}'\cdot\bar{\boldsymbol{e}})$	f′′
$-\left(\boldsymbol{c}'\cdot\hat{\boldsymbol{k}}'\right)(\boldsymbol{e}\cdot\boldsymbol{e})(\bar{\boldsymbol{e}}\cdot\bar{\boldsymbol{e}})$	g′′
$-\left(\boldsymbol{c}'\cdot\hat{\boldsymbol{k}}'\right)$	h′′
$\left(\hat{\boldsymbol{k}}'\times\bar{\boldsymbol{e}}'\cdot\bar{\boldsymbol{e}}\right)(\boldsymbol{e}'\cdot\bar{\boldsymbol{e}})(\boldsymbol{e}\cdot\boldsymbol{e})$	i′′

right-circularly polarized light and left-circularly polarized light. This scattered intensity difference, at a given angle θ (as in figure 4), is given by

$$\Delta I'(\theta) = I'_\theta(\mathrm{R}\to\eta') - I'_\theta(\mathrm{L}\to\eta'), \tag{15}$$

where η' is the polarization of the scattered light, which is most commonly measured for scattered light that is either polarized transverse $\perp$ or parallel $\parallel$ to $\hat{\boldsymbol{k}}'$.

The polarization unit vectors for circularly polarized light are defined as $\boldsymbol{e}^{(\mathrm{R/L})}(k\hat{\boldsymbol{z}}) = 2^{-1/2}(\boldsymbol{e}(\parallel;\hat{\boldsymbol{y}}) \mp i\boldsymbol{e}(\perp;\hat{\boldsymbol{x}}))$, such that $\boldsymbol{e}(\parallel)$, $\boldsymbol{e}(\perp)$ and $\hat{\boldsymbol{z}}$ form a right-handed orthogonal set, thus $\boldsymbol{c}^{(\mathrm{R/L})} = \boldsymbol{e}^{(\mathrm{R/L})}\times\bar{\boldsymbol{e}}^{(\mathrm{R/L})} = \pm i\hat{\boldsymbol{z}}$. In the scattering geometry in figure 4, for an input Laguerre–Gaussian beam that is circularly polarized, and the scattered light is resolved for either transverse or parallel polarization with respect to the output wave vector, the relevant optical products produced from those in tables 2–4 are shown in table 5. All of the other optical factors reduce to zero in this scenario because $\boldsymbol{c}' = \boldsymbol{e}'(\eta')\times\bar{\boldsymbol{e}}'(\eta') = 0$ for $\eta' = \perp/\parallel$, and $\boldsymbol{e}^{(\mathrm{R/L})}\cdot\boldsymbol{e}^{(\mathrm{R/L})} = 0$, $\bar{\boldsymbol{e}}^{(\mathrm{R/L})}\cdot\bar{\boldsymbol{e}}^{(\mathrm{R/L})} = 0$.

The results of table 5, when inserted into (15), give for the circular differential for scattered light that is polarized in the scattering plane as

$$\begin{aligned}\Delta I'(\parallel) = {}& \frac{N_r\bar{I}^2(r)\,g^{(2)}k^5}{16c\pi^2\varepsilon_0^3}\frac{1}{420}\left[\cos^3\theta\right.\\ &\{-20\mathrm{A}''-12\mathrm{B}''+60\mathrm{C}''-20\mathrm{D}''-12\mathrm{E}''\}+\cos^2\theta\\ &\{-4\mathrm{A}+16\mathrm{B}-4\mathrm{C}-52\mathrm{D}-4\mathrm{E}-16\mathrm{F}+28\mathrm{G}+2\mathrm{H}-16\mathrm{I}\}\\ &+\cos\theta\{16\mathrm{A}''-24\mathrm{B}''-48\mathrm{C}''+16\mathrm{D}''-24\mathrm{E}''\}\\ &+2\{-8\mathrm{A}+4\mathrm{B}-8\mathrm{C}+8\mathrm{D}+20\mathrm{E}-4\mathrm{F}-10\mathrm{H}-4\mathrm{I}\}\\ &+\frac{\ell}{kr}\sin 2\theta\cos\phi\{-6\mathrm{A}-4\mathrm{B}+8\mathrm{C}+36\mathrm{D}+8\mathrm{E}\\ &\left.+6\mathrm{F}-16\mathrm{G}-4\mathrm{H}+12\mathrm{I}\}\right],\end{aligned} \tag{16}$$

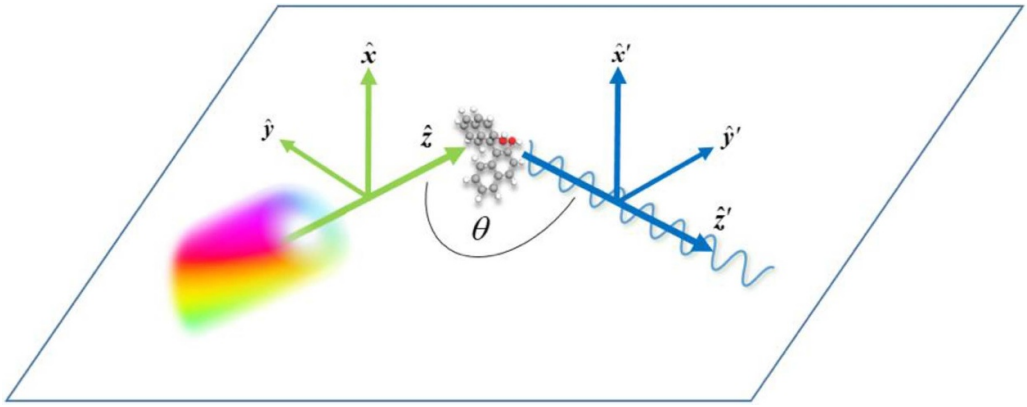

Figure 4. Schematic scattering geometry for the scattering of an input twisted light beam (colour of vortex represents helical phase) by a chiral molecule at an arbitrary angle θ. Primed quantities denote coordinates attached to the scattered light.

Table 5. Scattering angle dependence of the non-zero optical scalar invariants from tables 2–4 for input circularly polarized Laguerre–Gaussian light and scattered light polarized transverse to $\perp$ or in $\parallel$ the scattering $\hat{z}\hat{z}'$ plane according to the scattering geometry in figure 4. ϕ is the azimuthal angle associated with the input beam. (full derivation in SI).

Label	$\boldsymbol{e}^{(\mathrm{R/L})} \rightarrow \boldsymbol{e}'(\parallel)$	$\boldsymbol{e}^{(\mathrm{R/L})} \rightarrow \boldsymbol{e}'(\perp)$
a	$\pm i\left(1-\cos^2\theta\right)$	0
c	$\mp\frac{i}{2}\cos^2\theta$	$\mp\frac{i}{2}$
c′	$\mp\frac{i}{4}\sin 2\theta\,(i\sin\phi-\cos\phi)$	0
d′	$\pm\frac{i}{2}\sin 2\theta\cos\phi$	0
e′	$\mp\frac{i}{4}\sin 2\theta\,(i\sin\phi-\cos\phi)$	0
g′	$-\frac{1}{4}\sin 2\theta\,(\sin\phi\mp i\cos\phi)$	0
c′′	$\pm\frac{i}{2}\left(1-\cos^2\theta\right)\cos\theta$	0
d′′	$\pm\frac{i}{2}\left(1-\cos^2\theta\right)\cos\theta$	0
f′′	$\pm\frac{i}{2}\cos\theta$	$\pm\frac{i}{2}\cos\theta$

whereas for scattered light polarized transverse to the scattering plane the circular differential scattered intensity is

$$\Delta I'(\perp)=\frac{N_r\bar{I}^2(r)\,g^{(2)}k^5}{16c\pi^2\varepsilon_0^3}\frac{1}{420}\left[\cos\theta\{-\quad 4\mathrm{A}''-36\mathrm{B}''+12\mathrm{C}''\right.$$
$$-4\mathrm{D}''-36\mathrm{E}''\}+\{-20\mathrm{A}+24\mathrm{B}-20\mathrm{C}-36\mathrm{D}$$
$$\left.+36\mathrm{E}-24\mathrm{F}+28\mathrm{G}-18\mathrm{H}-24\mathrm{I}\}\right]. \tag{17}$$

The key finding of the analysis is contained in the final line of (16), which shows that hyper-Rayleigh (and Raman) scattered light can be dependent on the topological charge, i.e. the OAM of the beam, both its sign and magnitude. Evidently scattered light polarized transverse to the scattering plane (17) exhibits no OAM-dependence, and therefore the result (17) is almost the exact same as the well-known plane wave result [10], differing only through the input beam's radial intensity dependence. Indeed, if we set $\ell=0$ (and $p=0$), our equations would then be the result for an input Gaussian beam, which strongly mirrors the unstructured, plane wave description of hyper-Rayleigh and hyper-Raman optical activity.

It is instructive to draw out the similarities between the linear Rayleigh and Raman optical activity with twisted light recently derived [61, 62], and that of which we have derived here concerning the nonlinear Rayleigh and Raman optical activity. Firstly, in both cases there is no OAM-dependence for scattered light that is polarized transverse to the scattering plane. Secondly both exhibit an ℓ/kr dependent term with the same angle dependence of $\sin 2\theta$; this angle dependence is interesting in itself as it exhibits the intrinsic symmetry of a quadrupole. Furthermore, this different angle dependence for the terms dependent on the OAM of the incident photons, compared to the well-known 'plane wave' terms, offers a route to experimental verification of the mechanism via a judiciously placed polarization analyser. The ℓ/kr term highlights that this contribution to the circular differential changes sign if an $\ell>0$ input beam is switched to an $\ell<0$. As such, we may alternatively define a 'vortex differential' where we fix the circular polarization of the input beam and modulate between different topological charges—indeed, a recent technical breakthrough has shown how to modulate OAM beams [63].

It is also important to realize the mechanism is not only dependent on the sign of ℓ, but also its magnitude. The integer value of ℓ is theoretically unbounded, and although experimentally the OAM value of a twisted laser beam is restricted [64], large values are obtainable in relatively simple optical setups. The inverse radial distance dependence signifies that individual N_r molecules positioned closer to the centre of the beam contribute more significantly to this effect than those positioned further away; this is an intuitive outcome as it is well-known that the transverse gradients of the electric field are large in the optical vortex core. Spatially-dependent features are a well-known characteristic of light–matter interactions dependent on structured light.

Here it is worth clarifying an issue potentially not made clear in previous studies [46, 61, 65]. It is important to realise that the scattered signal is proportional to $\bar{I}^2(r)$ for hyper-Rayleigh and Raman optical activity specifically, and in general a vortex intensity distribution for any absorption/scattering process of twisted light, and therefore for light in the visible range of frequencies, the value of r necessary for the OAM-dependent scattered light to contribute significantly to the optical activity signal is well within the vortex core—it is roughly $r\approx\lambda$. As such, the signals will

more than likely not be measurable due to the almost zero intensity in this region for a typical Laguerre–Gaussian beam, unless the small fraction of molecules present essentially at the centre of the vortex give off large enough signals to be detected. There are, however, potential routes to obviate this issue. Firstly the importance of longitudinal fields for specific combinations of spin and orbital angular momentum, specifically $\ell = -\sigma$, may play a key factor for the very specific case of $|\ell| = 1$ as there is no longer an intensity null along the beam axis [66]. Using smaller wavelength light will allow focusing that generates a much smaller beam waist, on the scale of λ. X-ray optical vortices have been studied and shown to produce circular-vortex-dichroic absorption signals in cysteine molecules with respect to the sign of ℓ that are larger than standard circular dichroism with circularly polarized photons [67]. Furthermore, optical vortices with large beam waists have been generated [68] which possess an intensity pattern with a Gaussian envelope and a point singularity at the centre, leading to vortex core size to beam waist ratios of $w_{\mathrm{VC}}/w_0 \approx 0.02$. Another route, which has already been utilized to experimentally observe optical activity of twisted light [44], is the use of plasmonic enhancements of metallic nanoparticles to enhance the coupling between chiral molecules and optical vortex light [69]. Finally, plasmonic nanoantennas are currently being fabricated with the aim of breaking the diffraction limit for OAM light, and thus the generated vortices will be on a scale that matches molecular dimensions [70, 71].

The $\cos\phi$ dependence of OAM-dependent term leads to a vanishing result if a transverse beam profile average over 2π is carried out, i.e. the incident beam illuminates the whole material sample. Such a large spatial average is what has perhaps led to negative results in some of the initial experiments looking at the optical activity of twisted light [72]. This is easily obviated by an off-axis beam alignment or probing local sections of the output light. Trivially, the $\cos\phi$-dependence suggests that the maximum effect would be associated with only half the beam being incident on the material sample. The vanishing result of spatial averaging has its origins in the associated chirality of circularly polarized photons stemming from the polarization (a local property of the beam which does not vanish) and the orbital angular momentum which is a spatial or global property [73].

Finally, it is important to note that the use of twisted light versus unstructured light for a given input beam intensity should only serve to increase optical activity signals due to the fact it still produces the standard 'plane-wave' terms dependent on the M1 and the E2 axial field gradient, plus an additional term due to the E2 helical-phase gradient. The size of any such enhancement will be dependent on the experimental and optical parameters utilised, as discussed in the previous paragraphs.

5. Application to hyper-Raman scattering, selection rules, and molecular polarisability weightings

The above theory, although strictly applicable to hyper-Rayleigh scattering, can be easily adapted to account for hyper-Raman scattering using well established methods—for an explicit derivation of the method see [3]. The hyperpolarizability tensors in hyper-Rayleigh scattering and optical activity $\mathbf{\Pi}^{00} = \left\{\boldsymbol{\beta}^{00}, \boldsymbol{\chi}^{00}, \boldsymbol{\chi}'^{00}\right\}$ connect the initial ground electronic state to the final state, which itself is also the ground electronic state as no energy from the radiation field is imparted on the material in Rayleigh scattering. In the Raman effect both Stokes and anti-Stokes transitions occur, where for an initial $|i\rangle$ and final $|f\rangle$ molecular state the conservation of energy of the process is given by $E_{fi} = \hbar(2\omega_k - \omega'_{k'})$. In Raman processes we are generally concerned with $|f\rangle \leftarrow |i\rangle$ leading to an identical initial and final electronic state, but a different vibrational state $|V\rangle$. The derivation of the scattered intensity (11) for hyper-Raman scattering and optical activity is of an exactly parallel form to that of the hyper-Rayleigh case, except the molecular tensors now become $\mathbf{\Pi}^{fi} = \left\{\boldsymbol{\beta}^{fi}, \boldsymbol{\chi}^{fi}, \boldsymbol{\chi}'^{fi}\right\}$, allowing us to accommodate stokes and anti-stokes transitions. The general result can be made much simpler by assuming the Born–Oppenheimer approximation, and that the incident laser light and the scattered harmonic are far removed from resonance (though resonance can be accounted for withint the theory if necessary), as then the hyper-Raman polarizability tensors can be approximated as

$$\mathbf{\Pi}^{FI}(-2\omega;\omega,\omega) \approx \langle F(0)|\,\mathbf{\Pi}^{00}(-2\omega;\omega,\omega)\,|I(0)\rangle \qquad (18)$$

where $\mathbf{\Pi}^{00}$ is the corresponding electronic hyperpolarizability which involves the sum over intermediate electronic states; $|I(0)\rangle$ and $|F(0)\rangle$ are initial I and final F vibrational states connected to the ground electronic state 0. The electronic wavefunctions in (18) are sensitive to nuclear geometry and the hyperpolarizability tensors themselves are connected to a nuclear coordinate Q_j . This allows (18) to be expanded in the following Taylor series around the vibrational coordinates Q:

$$\langle F(0)|\,\mathbf{\Pi}^{00}(Q_j)\,|I(0)\rangle = \mathbf{\Pi}^{00}(Q_e)\,\langle F(0)|\,I(0)\rangle + \left.\frac{\partial \mathbf{\Pi}^{00}}{\partial Q_j}\right|_{Q_e} \langle F(0)|\,Q_j - Q_e\,|I(0)\rangle + \cdots, \qquad (19)$$

where Q_e is the equilibrium configuration. The first term in (19) is non-zero only when $I(0) = F(0)$ and the molecule has a non-zero hyperpolarizability $\mathbf{\Pi}^{00}(Q_e)$ in its equilibirum nuclear configuration: this first term therefore represents the dominant contribution to hyper-Rayleigh scattering and optical activity. The second term in (19) represents the leading contribution to hyper-Raman scattering and optical activity, with higher-order terms producing overtones. The gross selection rules for hyper-Raman optical activity with twisted light can thus be derived in the exact same manner as is standard [74]: The partial derivative in the second term of (19) must be non-zero, and therefore $\mathbf{\Pi}^{00}$ must change during vibration as the molecule passes through its equilibrium configuration; and the $\langle F(0)|\,Q_j - Q_e\,|I(0)\rangle$ bra-ket leads to the usual vibrational selection rule $F = I \pm 1$. The first rule also signifies that although a non-zero $\mathbf{\Pi}^{00}(Q_e)$ is required in hyper-Rayleigh scattering and optical activity, in the case of hyper-Raman scattering and optical activity it must only have a non-zero

value for $\partial\boldsymbol{\Pi}^{00}/\partial Q_j$, and so molecules that exhibit no hyper-Rayleigh scattering/optical activity may still engage in hyper-Raman scattering/optical activity (which is not the case for linear scattering).

Clearly the use of paraxial Laguerre–Gaussian light does not influence the basis of gross selection rules in isotropic molecular systems as is to be expected: selection rules originate in material structure. Rather, it produces modified transition probabilities (or scattering cross sections) which depend on various parameters linked to the optical part of the system—position within the beam, OAM content, and the weightings of the molecular invariants (which stem from the polarization products in tables 3 and 5). Similarly, it has been highlighted that forward Raman scattering in cubic crystals with optical vortices leads to the activation of usually silent phonon modes [75] and transition probabilities for the absorption of twisted photons by atoms have been experimentally proven to be significantly position-dependent [76]. With specific regards to the results of this work, the relative contributions from different orientationally averaged, scalar molecular polarizability invariants (A–E in table 1) are significantly influenced by the incident optical vortex structure. This is a unique property of nonlinear optical activity with twisted photons compared to linear optical activity counterparts [61, 62]. In the previous Section the similarities between linear and nonlinear optical activity with twisted light were discussed, where it was noted that they depend on the same optical parameters. The ℓr^{-1}-dependent circular-vortex *linear* differential scattering contribution to the overall differential effect in *linear* optical activity occurs through the exact same weighted molecular scalar invariant as the standard OAM-independent analogous circular-differential scattering:$\varepsilon_{\lambda\alpha\beta}\alpha_{\lambda\mu}A_{\alpha\beta\mu}$. However, it is clear in the bottom line of (16) that the weightings of the different molecular invariants A-E are significantly different to the weightings of A-E in the scattering angle independent, and $\cos^2\theta$, terms. This leads to a significantly expanded scope of experimental ability to probe different molecular parameters and the verification of nonlinear optical activity with twisted light. One of the many potentially interesting scenarios is for the specific situation when scattering occurs at $\sin 2\theta = \cos^2\theta$ and $\ell/kr = 1$, the total contribution from the D terms is zero; however, reversal of the topological charge of the input beam, i.e. $\ell = -1$ and the D contributions double in magnitude compared to the plane wave case. Detailed selection rules for any specific molecule for our results can be obtained in the usual way through group theory and irreducible representations, the complete reduction of fourth-rank Cartesian tensors being readily available [77].

6. Conclusion

It has been shown that hyper-Rayleigh and hyper-Raman scattering of twisted light by chiral molecules is dependent on the handedness of the helical wavefront of an optical vortex. That is, nonlinear scattering by chiral molecules is dependent on the OAM content of photons, both their sign and magnitude. It has been highlighted that the optical vortex structure of the input beam affords transition probabilities and scattered intensities dependent on parameters unique to optical vortices and twisted photons; a route to increase the nonlinear optical activity signals; and the ability to probe chiral molecular structure that has been previously unavailable in both linear scattering and nonlinear scattering methods using unstructured light sources. The end of section 4 highlights some potential methods and scenarios of observing these effects in experiments. It is clear that the field of optical activity and twisted light will provide experimentalists with plenty of scope to produce many novel techniques in the pursuit of the added layer of richness that using structured light in spectroscopy has the potential to provide.

This is the first study on nonlinear optical activity of twisted light to our knowledge. It is anticipated that the general principles outlined here will apply to further nonlinear twisted light optical activity phenomena, and such chiroptical effects due to the OAM of light should manifest in two-photon circular dichroism, for example. Future directions this specific work could be expanded into include studying circular polarization differences in the scattered light or both the incident and scattered light [78]; more novel would be detecting specific scattered OAM modes [79]. With the experimental observation of both hyper-Rayleigh optical activity with unstructured laser light [26, 27] and optical activity with twisted light [44] very recently secured, it is hoped that this work stimulates nonlinear spectroscopy techniques to be developed which incorporate the unique properties of twisted light.

Acknowledgments

K A F would like to thank Professor David L Andrews for comments on the manuscript, constant encouragement, and generously supplying original notes on three-dimensional rotational averages that aided with calculations involved in the seventh-rank rotational averaging; Dale Green for help constructing figure 2; and the Leverhulme Trust for funding through a Leverhulme Early Career Fellowship (ECF-2019-398).

ORCID iD

Kayn A Forbes https://orcid.org/0000-0002-8884-3496

References

[1] Andrews D L 2015 *Photonics, Volume 1: Fundamentals of Photonics and Physics* (New York: Wiley)
[2] Gu B, Zhao C, Baev A, Yong K-T, Wen S and Prasad P N Molecular nonlinear optics: recent advances and applications 2016 *Adv. Opt. Photonics* **8** 328
[3] Andrews D L and Allcock P 2002 *Optical Harmonics in Molecular Systems: Quantum Electrodynamical Theory* (Weinheim: Wiley)
[4] Andrews D L and Thirunamachandran T The hyper-raman effect: a new approach to vibrational mode classification and assignment of spectral lines 1978 *J. Chem. Phys.* **68** 2941–51
[5] Campo J, Desmet F, Wenseleers W and Goovaerts E 2009 Highly sensitive setup for tunable wavelength

hyper-Rayleigh scattering with parallel detection and calibration data for various solvents *Opt. Express* **17** 4587–604
[6] Andrews D L and Blake N P 1988 Forbidden nature of multipolar contributions to second-harmonic generation in isotropic fluids *Phys. Rev.* A **38** 3113
[7] Russier-Antoine I, Bertorelle F, Vojkovic M, Rayane D, Salmon E, Jonin C, Dugourd P, Antoine R and Brevet P-F 2014 Non-linear optical properties of gold quantum clusters. The smaller the better *Nanoscale* **6** 13572–8
[8] Tocci G, Liang C, Wilkins D M, Roke S and Ceriotti M 2016 Second-harmonic scattering as a probe of structural correlations in liquids *J. Phys. Chem. Lett.* **7** 4311–6
[9] Rodriquez M B and Shelton D P 2018 What is measured by hyper-Rayleigh scattering from a liquid? *J. Chem. Phys.* **148** 134504
[10] Andrews D L and Thirunamachandran T 1979 Hyper- Raman scattering by chiral molecules *J. Chem. Phys.* **70** 1027–30
[11] Andrews D L 2018 Quantum formulation for nanoscale optical and material chirality: symmetry issues, space and time parity, and observables *J. Opt.* **20** 033003
[12] Barron L D 2009 *Molecular Light Scattering and Optical Activity* (Cambridge: Cambridge University Press)
[13] Berova N, Polavarapu P L, Nakanishi K and Woody R W 2011 *Comprehensive Chiroptical Spectroscopy: Instrumentation, Methodologies, and Theoretical Simulations* vol 1 (New York: Wiley)
[14] Berova N, Polavarapu P L, Nakanishi K and Woody R W 2012 *Comprehensive Chiroptical Spectroscopy: Applications in Stereochemical Analysis of Synthetic Compounds, Natural Products, and Biomolecules* vol 2 (New York: Wiley)
[15] Barron L D and Buckingham A D 2010 Vibrational optical activity *Chem. Phys. Lett.* **492** 199–213
[16] Nafie L A 2011 *Vibrational Optical Activity: Principles and Applications* (New York: Wiley)
[17] Barron L D 2015 The development of biomolecular Raman optical activity spectroscopy *Biomed. Spectrosc. Imaging* **4** 223–53
[18] Barron L D, Mutter S T and Blanch E W 2018 Raman optical activity *Chiral Analysis: Advances in Spectroscopy, Chromatography and Emerging Methods* (Amsterdam: Elsevier) pp 249–91
[19] Verbiest T, Clays K and Rodriguez V 2009 *Second-Order Nonlinear Optical Characterization Techniques: An Introduction* (Boca Raton, FL: CRC Press)
[20] Fischer P and Hache F 2005 Nonlinear optical spectroscopy of chiral molecules *Chirality* **17** 421–37
[21] Chung C-Y J and Potma E O 2013 Biomolecular imaging with coherent nonlinear vibrational microscopy *Annu. Rev. Phys. Chem.* **64** 77–99
[22] Okuno M and Ishibashi T 2014 Chirality discriminated by heterodyne-detected vibrational sum frequency generation *J. Phys. Chem. Lett.* **5** 2874–8
[23] Yan E C, Fu L, Wang Z and Liu W 2014 Biological macromolecules at interfaces probed by chiral vibrational sum frequency generation spectroscopy *Chem. Rev.* **114** 8471–98
[24] Chen M-Y, Huttunen M J, Kan C-W, Deka G, Lin -Y-Y, Ye C-W, Wu M-J, Liu H-L and Chu S-W 2018 Resonant nonlinear microscopy reveals changes in molecular level chirality in native biological tissues *Opt. Commun.* **422** 56–63
[25] Rodrigues S P, Lan S, Kang L, Cui Y and Cai W Nonlinear imaging and spectroscopy of chiral metamaterials 2014 *Adv. Mater.* **26** 6157–62
[26] Collins J T, Rusimova K R, Hooper D C, Jeong -H-H, Ohnoutek L, Pradaux-Caggiano F, Verbiest T, Carbery D R, Fischer P and Valev V K 2019 First observation of optical activity in hyper-Rayleigh scattering *Phys. Rev.* X **9** 011024
[27] Verreault D, Moreno K, Merlet E, Adamietz F, Kauffmann B, Ferrand Y, Olivier C and Rodriguez V 2019 hyper-Rayleigh scattering as a new chiroptical method: uncovering the nonlinear optical activity of aromatic oligoamide foldamers *J. Am. Chem. Soc.* **142** 257–63
[28] Marble C B, Xu X, Keppler M, Gil E, Petrov G I, Wang D and Yakovlev V V 2020 hyper-Raman optical activity of biologically relevant chiral molecules *Proc. SPIE* **11288** 1128829
[29] Allen L, Beijersbergen M W, Spreeuw R J C and Woerdman J P 1992 Orbital angular momentum of light and the transformation of Laguerre–Gaussian laser modes *Phys. Rev.* A **45** 8185–9
[30] Andrews D L and Babiker M 2012 *The Angular Momentum of Light* (Cambridge: Cambridge University Press)
[31] Barnett S M, Babiker M and Padgett M J 2017 *Optical Orbital Angular Momentum* (London: The Royal Society)
[32] Rubinsztein-Dunlop H *et al* 2016 Roadmap on structured light *J. Opt.* **19** 013001
[33] Andrews D L (Ed.) 2011 *Structured Light and Its Applications: An Introduction to Phase-Structured Beams and Nanoscale Optical Forces* (New York: Academic)
[34] Willner A E, Huang H, Yan Y, Ren Y, Ahmed N, Xie G, Bao C, Li L, Cao Y and Zhao Z 2015 Optical communications using orbital angular momentum beams *Adv. Opt. Photonics* **7** 66–106
[35] Babiker M, Andrews D L and Lembessis V E 2018 Atoms in complex twisted light *J. Opt.* **21** 013001
[36] Lee J, Arita Y, Toyoshima S, Miyamoto K, Panagiotopoulos P, Wright E M, Dholakia K and Omatsu T Photopolymerization with light fields possessing orbital angular momentum: generation of helical microfibers 2018 *ACS Photonics* **5** 4156–63
[37] Fickler R, Campbell G, Buchler B, Lam P K and Zeilinger A 2016 Quantum entanglement of angular momentum states with quantum numbers up to 10,010 *Proc. Natl Acad. Sci.* **113** 13642–7
[38] Chaitanya N A, Jabir M V and Samanta G K 2016 Efficient nonlinear generation of high power, higher order, ultrafast 'perfect' vortices in green *Opt. Lett.* **41** 1348–51
[39] Li Y, Zhou Z-Y, Liu S-L, Liu S-K, Yang C, Xu Z-H, Li Y-H and Shi B-S 2019 Frequency doubling of twisted light independent of the integer topological charge *OSA Contin.* **2** 470
[40] Walker G, Arnold A S and Franke-Arnold S 2012 Trans-spectral orbital angular momentum transfer via four-wave mixing in Rb vapor *Phys. Rev. Lett.* **108** 243601
[41] Coles M M, Williams M D and Andrews D L 2013 Second harmonic generation in isotropic media: six-wave mixing of optical vortices *Opt. Express* **21** 12783–9
[42] Zhang D, Liu X, Yang L, Li X, Zhang Z and Zhang Y 2017 Modulated vortex six-wave mixing *Opt. Lett.* **42** 3097–100
[43] van Veenendaal M and McNulty I 2007 Prediction of strong dichroism induced by x-rays carrying orbital momentum *Phys. Rev. Lett.* **98** 157401
[44] Brullot W, Vanbel M K, Swusten T and Verbiest T 2016 Resolving enantiomers using the optical angular momentum of twisted light *Sci. Adv.* **2** e1501349
[45] Afanasev A, Carlson C E and Solyanik M 2017 Circular dichroism of twisted photons in non-chiral atomic matter *J. Opt.* **19** 105401
[46] Forbes K A and Andrews D L 2018 Optical orbital angular momentum: twisted light and chirality *Opt. Lett.* **43** 435–8
[47] Reddy I V, Baev A, Furlani E P, Prasad P N and Haus J W 2018 Interaction of structured light with a chiral plasmonic

metasurface: giant enhancement of chiro-optic response *ACS Photonics* **5** 734–40
[48] Craig D P and Thirunamachandran T 1998 *Molecular Quantum Electrodynamics: An Introduction to Radiation-Molecule Interactions* (New York: Courier Corporation)
[49] Salam A 2010 *Molecular Quantum Electrodynamics: Long-Range Intermolecular Interactions* (New York: Wiley)
[50] Andrews D L, Bradshaw D S, Forbes K A and Salam A 2020 Quantum electrodynamics in modern optics and photonics: tutorial *J. Opt. Soc. Am.* B **37** 1153–72
[51] Andrews D L, Jones G A, Salam A and Woolley R G 2018 Perspective: quantum hamiltonians for optical interactions *J. Chem. Phys.* **148** 040901
[52] Romero L D, Andrews D L and Babiker M 2002 A quantum electrodynamics framework for the nonlinear optics of twisted beams *J. Opt. B: Quantum Semiclass. Opt.* **4** S66–72
[53] Andrews D L, Romero L D and Babiker M 2004 On optical vortex interactions with chiral matter *Opt. Commun.* **237** 133–9
[54] Mathevet R, de Lesegno B V, Pruvost L and Rikken G L 2013 Negative experimental evidence for magneto-orbital dichroism *Opt. Express* **21** 3941–5
[55] Andrews D L 2011 Structured light transmission, and scattering *Proc. SPIE* **7950** 79500L
[56] Forbes K A and Salam A 2019 Kramers-Heisenberg dispersion formula for scattering of twisted light *Phys. Rev.* A **100** 053413
[57] Babiker M, Bennett C R, Andrews D L and Romero L D 2002 Orbital angular momentum exchange in the interaction of twisted light with molecules *Phys. Rev. Lett.* **89** 143601
[58] Schmiegelow C T and Schmidt-Kaler F 2012 Light with orbital angular momentum interacting with trapped ions *Eur. Phys. J.* D **66** 157–66
[59] Fischer P and Salam A 2010 Molecular QED of coherent and incoherent sum-frequency and second-harmonic generation in chiral liquids in the presence of a static electric field *Mol. Phys.* **108** 1857–68
[60] Andrews D L and Thirunamachandran T 1977 On three-dimensional rotational averages *J. Chem. Phys.* **67** 5026–33
[61] Forbes K A Raman optical activity using twisted photons 2019 *Phys. Rev. Lett.* **122** 103201
[62] Forbes K A and Andrews D L 2019 Enhanced optical activity using the orbital angular momentum of structured light *Phys. Rev. Res.* **1** 033080
[63] Bisson J-F, Miyamoto K and Omatsu T 2019 Power-scalable and high-speed orbital angular momentum modulator *Japan J. Appl. Phys.* **58** 032009
[64] Roux F S 2003 Optical vortex density limitation *Opt. Commun.* **223** 31–7
[65] Forbes K A and Andrews D L 2019 Spin-orbit interactions and chiroptical effects engaging orbital angular momentum of twisted light in chiral and achiral media *Phys. Rev.* A **99** 023837
[66] Bliokh K Y, Rodríguez-Fortuño F J, Nori F and Zayats A V 2015 Spin–orbit interactions of light *Nat. Photonics* **9** 796–808
[67] Ye L, Rouxel J R, Asban S, Rösner B and Mukamel S 2019 Probing molecular chirality by orbital angular momentum carrying x-ray pulses *J. Chem. Theory Comput.* **15** 4180–6
[68] Rumala Y S and Leanhardt A E 2017 Optical vortex with a small core and gaussian intensity envelope for light-matter interaction *J. Opt. Soc. Am.* B **34** 909–18
[69] Wu T, Wang R and Zhang X 2015 Plasmon-induced strong interaction between chiral molecules and orbital angular momentum of light *Sci. Rep.* **5** 18003
[70] Arikawa T, Morimoto S and Tanaka K 2017 Focusing light with orbital angular momentum by circular array antenna *Opt. Express* **25** 13728–35
[71] Shutova M, Shutov A D and Sokolov A V 2020 Spectroscopic sensing enhanced by quantum molecular coherence and by plasmonic nanoantennas *Proc. SPIE* **11296** 1129605
[72] Löffler W, Broer D J and Woerdman J P 2011 Circular dichroism of cholesteric polymers and the orbital angular momentum of light *Phys. Rev.* A **83** 065801
[73] Allen L and Padgett M 2007 Equivalent geometric transformations for spin and orbital angular momentum of light *J. Mod. Opt.* **54** 487–91
[74] Hollas J M 2004 *Modern Spectroscopy* (New York: Wiley)
[75] Li J, Tu J J and Birman J L 2015 Raman scattering using vortex light *J. Phys. Chem. Solids* **77** 117–21
[76] Afanasev A, Carlson C E, Schmiegelow C T, Schulz J, Schmidt-Kaler F and Solyanik M 2018 Experimental verification of position-dependent angular-momentum selection rules for absorption of twisted light by a bound electron *New J. Phys.* **20** 023032
[77] Andrews D L and Ghoul W A 1982 Irreducible fourth-rank cartesian tensors *Phys. Rev.* A **25** 2647
[78] Li H and Nafie L A 2012 Simultaneous acquisition of all four forms of circular polarization Raman optical activity: results for α-pinene and lysozyme *J. Raman Spectrosc.* **43** 89–94
[79] Paroli B, Siano M and Potenza M A C The local intrinsic curvature of wavefronts allows to detect optical vortices 2019 *Opt. Express* **27** 17550–60